MODELLING OF THE DELAMINATION AND FIBER-BRIDGING IN UNIDIRECTIONAL COMPOSITES UNDER MODE-I LOADING CONDITIONS

András Szekrényes

Budapest University of Technology and Economics, Budapest, Hungary

ABSTRACT

The DCB test for mode-I loading was utilized to obtain the interlaminar fracture toughness of two type of CFRP composites. Elastic theoretical and finite element analyses were conducted to model the R-curve behavior of laminated composites. In the theory, the bridging fibers were represented by elastic beams, while the stress field behind the crack-tip was calculated from the elastic foundation model. In the FE analysis the bridging fibers were modeled with TRUSS2D beam elements. The fracture toughness was evaluated numerically by the path independent J-integral. The analysis was done by the finite element code COSMOS/M 2.0. Experimental results were used from previous publications and comparison was made with the current computations. Comparison in the results shows, in the theory it is necessary to consider the fiber-bridging and the elastic foundation to obtain reasonably good, fully analytical values for the fracture energy. On the other hand, the FE models overpredict the mode-I toughness in the final stage of crack propagation. Simulating the bridging fibers these overpredictions can be eliminated.

1. INTRODUCTION

In the recent years the interlaminar fracture toughness of composite materials is very intensively investigated by designers. The theoretical foundation, as well as experimental and finite element analysis is very important to know thoroughly the delamination process in composite materials. The interlaminar fracture toughness can be affected by many parameters (e.g.: material properties, loading speed, temperature, data reduction scheme). Several authors reported the R-curve behavior of laminated composites measured experimentally under mode-I loading conditions [1,2]. The R-curve behavior is mainly attributed to the fiber-bridging process, which enhances the resistance to delamination. The fiber-bridging occurs only under mode-I (opening mode) and mixed-mode I+II (opening and in-plane shearing mode) loading conditions. The double cantilever beam (DCB) specimen is the most commonly used to investigate the mode-I fracture properties of laminated composites. In literature the elastic beam theory is used as data reduction scheme for the fracture toughness test of composite materials. The results of the linear elastic beam theory often disagree with the experimentally measured fracture toughness. In fact the beam theory, denoted as global method should be completed with other factors, which account the effects of block stiffness, frictional forces and other testing conditions. The corrected beam theory (CBT) counts for the large displacement block stiffening and crack-tip rotation and deflection [2,3]. Plotting the crack length against the third root of the compliance results the Δ-correction of the crack length. The classical beam theory assumes that the arms of

the DCB specimen are rigidly built-in in the uncracked region of the specimen. Ozdil and Carlsson presented a study about unidirectional and angle-ply E-glass/polyester DCB specimens using the Winkler foundation model, a fourth order differential equation for the deflection function of the DCB specimen [1]. The study completed the results of the elementary beam theory with a power factor, which depends on the first, second and the third root of the crack length and the moduli ratio (E_x/E_z). Using the former factors the experimental results can be followed with more accuracy. The finite element method is widely acknowledged by designers, denoted as local method. The virtual clack closure technique (VCCT), or commonly known as the modified clack closure integral (MCCI) uses the nodal displacements and forces in the vicinity of the crack-tip to calculate the strain energy release rate. This method is suitable for four- and eight-noded plane stress and plane strain models as well as for three-dimensional ones [4]. The J-integral is also a local method, which depends on the opening angle and the stress field around the crack-tip. The J-integral is applicable only for isotropic plane stress and plane strain models [5]. Both the beam theory and the finite element analysis require the experimentally measured force/crack opening displacement (P-δ) curves as input data. The experimental studies often report fiber-bridging and crossing fibers along the delamination front [6,7]. These fibers increase the resistance to delamination. Hence the force/displacement curves include the bridging and breakage of fibers through the delamination process.

This study presents theoretical and finite element analyses of the DCB specimen based on the experimental research work of Morais et al. and Hashemi et al. [2,6]. Unidirectional carbon/epoxy and carbon/polyether-ether ketone (PEEK) composite properties were utilized. Experimentally measured force/displacement curves were used as input in the analysis. The main goal of this study is to identify discrepancies in the experimental and theoretical values of the fracture toughness based on the fiber-bridging phenomenon and the elastic foundation of the uncracked region.

2. DETERMINATION OF THE FRACTURE TOUGHNESS

2.1. Beam theory.

The fracture toughness can be determined using the formulas of the Euler-Bernoulli beam theory as shown in Fig.1.

Specimen design	*Compliance*	*Fracture toughness*
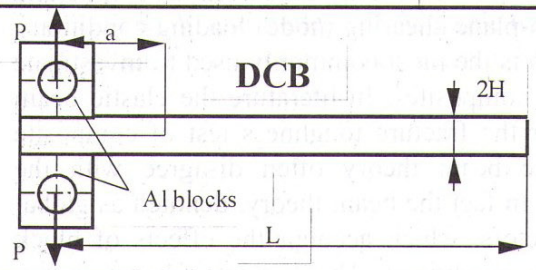	$C = \frac{8a^3}{WH^3E_x}$	$G_I = \frac{12P^2a^2}{W^2H^3E_x}$ $G_I = \frac{3P\delta}{2Wa}$

Fig.1. Compliance and interlaminar fracture toughness for the mode-I DCB specimen.

In this theory the composite specimens are considered as homogeneous elastic beams [8]. The general Irwin-Kies expression calculates the fracture toughness using the compliance of the specimen [9]:

$$G_I = \frac{P^2}{2W}\frac{dC}{da}, \tag{1}$$

where P is load, C is the compliance, W is specimen width and a is the actual crack length.

2.2. J-integral.

The interlaminar fracture toughness (G_I) was calculated by the J-integral in this study. The J-integral is equivalent with the fracture toughness undergoing small strains under quasi-static conditions. The expression for the J-integral [5,9]:

$$J = \int_g \left(W dy - T_i \frac{\partial u_i}{\partial x} ds \right), \tag{2}$$

where g is arbitrary contour around the crack tip, W is the total strain energy density, T_i are the components of traction vector, u_i are the components of displacement vector and ds is the arc length along the contour g. The J-integral is applicable only for isotropic, plane strain and plane stress models.

3. THEORETICAL ANALYSIS OF THE FIBER-BRIDGING

In this section we establish a new approximation for the fiber-bridging phenomenon based on elastic beam theory. The beam analysis was conducted using the following assumptions:

- the crack length has the same size in both sides of the specimen;
- the upper and lower arms of the specimen behave as rigidly built-in in the uncracked region of the beam with zero slope and displacement at the crack-tip;
- the fiber-bridging occurs only in the final stage of the delamination process;
- the displacement and force components in the x direction were neglected in the theory;
- since the displacement function depends on the P_{r1} force (Fig.2a.), the crack opening displacement (COD) in the loading point was calculated from the beam analysis, the force was read from the experimental force/displacement curves;
- stable crack growth was assumed in every crack length.

Considering the DCB specimen in Fig.2a, which has two region due to the bridging fiber and expressing the bending moment functions for the upper and lower arms of the specimen:

$$M_{u1}(x) = -Px, \qquad M_{u2}(x) = -Px + P_{r1}(x - l_1), \tag{3}$$

$$M_{l1}(x) = Px, \qquad M_{l2}(x) = Px - P_{r1}(x - l_2). \tag{4}$$

The strain energy from the bending moment functions can be calculated for the upper and lower arms as follows:

$$U_u = \frac{1}{2}\int_0^{l_1} \frac{M_{u1}^{\ 2}}{I_y E_x} dx + \frac{1}{2}\int_{l_1}^{a} \frac{M_{u2}^{\ 2}}{I_y E_x} dx, \tag{5}$$

$$U_l = \frac{1}{2}\int_0^{l_2} \frac{M_{l1}^{\,2}}{I_y E_x}\,dx + \frac{1}{2}\int_{l_2}^{a} \frac{M_{l2}^{\,2}}{I_y E_x}\,dx\,. \tag{6}$$

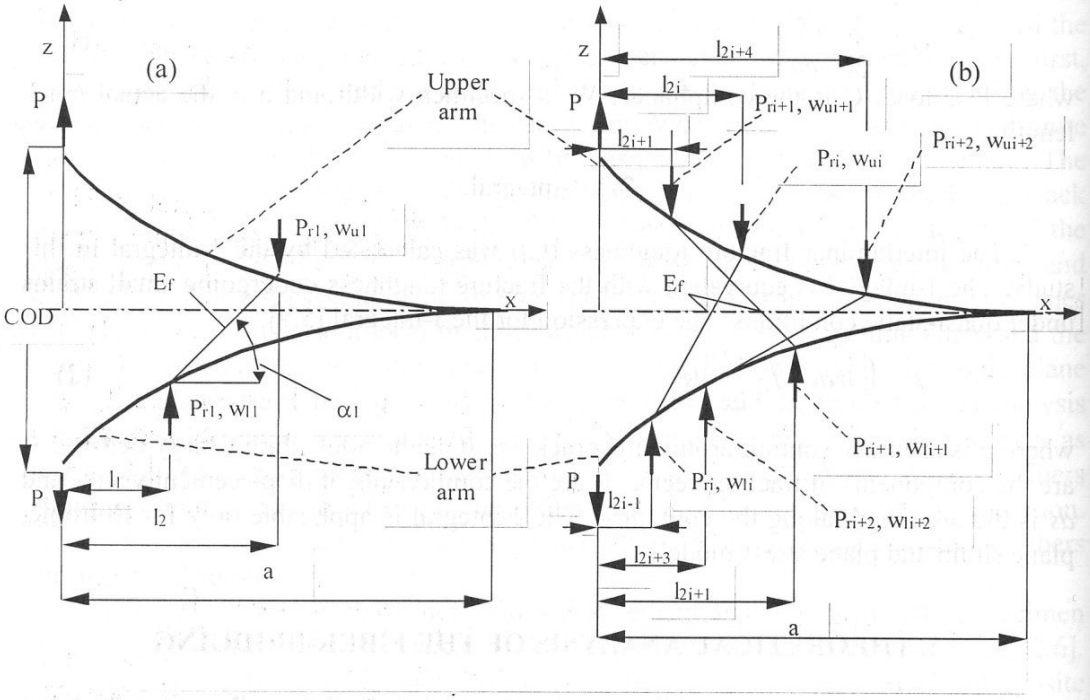

Fig.2. Elastic analysis of the fiber-bridging in the DCB specimen.

First we calculate the displacement in the bridging fibers by expressing the displacements at l_1 and l_2:

$$w_{u1} = \frac{\partial U_u}{\partial P_{r1}}, \qquad w_{l1} = \frac{\partial U_l}{\partial P_{r1}}. \tag{7}$$

It was assumed that the bridging fiber is connected to the arms with pins. According to this the elongation in the bridging fiber:

$$\Delta r_1 = \sqrt{\left[w_{u1} + w_{l1}\right]^2 + l_{01}^{\,2}} - l_{01}, \tag{8}$$

where $l_{01}=l_2-l_1$ is the initial length of the debonded fiber. The tensile force in the bridging fiber:

$$F_{r1} = s_1 \Delta r_1, \; s_1 = \frac{A_1 E_f}{l_{01}}, \tag{9}$$

where s is the stiffness, A_1 is the cross-section of the bridging fiber. The next step is to express the offaxis angle between the bridging fiber and the x-axis:

$$\alpha_1 = \arctan\left(\frac{w_{u1} + w_{l1}}{l_2 - l_1}\right). \tag{10}$$

Hence the force P_{r1} which loads the DCB specimen, according to Fig.2a:

$$P_{r1} = F_{r1} \sin\alpha_1\,. \tag{11}$$

Substituting Eq.(8), Eq.(9) and Eq.(10) into the expression of P_{r1} and substituting the displacements in Eq.(7) into the formula of α_1 in Eq.(10) yields a transcendent equation, which can be solved for P_{r1} by a numerical procedure. In fact in the case of fiber-bridging several debonded fiber bundles can be observed as reported and photographed

by several authors [7,10,11]. The location and the length of the bridging fiber bundles should be determined from experiments. According to this in Fig.2b it was assumed that the number of bridging fiber bundles is 'i'. The displacement function depends on the location of the connection between the bridging fiber and the DCB specimen. Similarly, using the beam stiffnesses (s_i, s_{i+1}, s_{i+2}) and expressing the tensile forces and the offaxis angles an equation system is resulted, which should be solved numerically for P_{ri}, P_{ri+1}, P_{ri+2}. In this study the former numerical procedure was conducted by using the code Maple V Release 5 [12]. After the equation system has been solved for the forces the compliance of the specimen can be expressed using Castigliano's principle:

$$C = \frac{1}{P}\frac{\partial U}{\partial P} = \frac{8a^3}{WH^3E_x} - \frac{[2P_{r1}(4a^3 - 3l_1a^2 - 3l_2a^2 + l_1^{\,3} + l_2^{\,3})]}{PWH^3E_x}, \tag{12}$$

where $U=U_u+U_l$ the strain energy for the upper and lower arms of the DCB specimen. The two forms of the fracture energy can be obtained by using Eq.(1):

$$G_I = \frac{12P^2a^2}{W^2H^3E_x} - \frac{6Pa[P_{r1}(2a - l_1 - l_2)]}{W^2H^3E_x}, \tag{13}$$

the another form containing the COD:

$$G_I = \frac{3P\delta a[2Pa - P_{r1}(2a - l_1 - l_2)]}{W[4Pa^3 - P_{r1}(4a^3 - 3l_1a^2 - 3l_2a^2 + l_1^{\,3} + l_2^{\,3})]}. \tag{14}$$

In Eq.(13) it can be noticed that the first term is the well-known formula from elastic beam theory, the second term arises only if fiber-bridging occurs. Eq.(13) is valid only for one bridging fiber bundle. In Eq.(14), if P_{r1} vanishes, we get back the formula of the simple beam theory. The former procedure was used for several cases including symmetrical and asymmetrical arrangements of the fiber-bridging form. The results for these cases are summarized in Fig.3. As the summary of the results, the following generalized closed-formed expressions can be derived for the compliance:

$$C = \frac{8a^3}{H^3WE_x} - \sum_i^n \frac{\beta \cdot 2P_{ri}}{P}\left(\frac{4a^3 - 3a^2(l_{2i-1} + l_{2i}) + l_{2i-1}^{\,3} + l_{2i}^{\,3}}{H^3WE_x}\right), \tag{15}$$

and for the fracture toughness:

$$G_I = \frac{12P^2a^2}{W^2H^3E_x} - \sum_{i=1}^n \frac{6\beta \cdot Pa[P_{ri}(2a - l_{2i-1} - l_{2i})]}{W^2H^3E_x}, \tag{16}$$

$$G_I = \frac{3P\delta a\left[\gamma \cdot Pa - \sum_{i=1}^n P_{ri}(2a - l_{2i-1} - l_{2i})\right]}{W\left[2\gamma \cdot Pa^3 - \sum_i^n P_{ri}\left(4a^3 - 3a^2(l_{2i-1} + l_{2i}) + l_{2i-1}^{\,3} + l_{2i}^{\,3}\right)\right]}, \tag{17}$$

where $\beta=2$, $\gamma=1$ for symmetric arrangement and $\beta=1$, $\gamma=2$ for asymmetric arrangements and n is the number of distinct forces due to fiber-bridging, acting on the arms of the DCB specimen. It must be pointed out, that for determining the forces P_{ri} a numerical solution is required due to the transcendent equation system. In this study the location of bridging fibers were chosen arbitrarily, but publications, which has reported fiber-bridging were used to compare the analytical and experimental results.

Fiber-bridging form	*Compliance and mode-I fracture toughness*
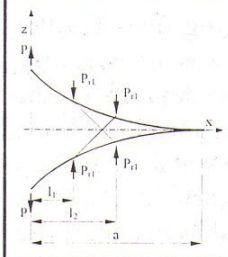	$C = \frac{8a^3}{WH^3E_x} - \frac{4[P_{r1}(4a^3 - 3l_1a^2 - 3l_2a^2 + l_1^3 + l_2^3)]}{PWH^3E_x}$ $G_I = \frac{12P^2a^2}{W^2H^3E_x} - \frac{12Pa[P_{r1}(2a - l_1 - l_2)]}{W^2H^3E_x}$ $G_I = \frac{3P\delta a[Pa - P_{r1}(2a - l_1 - l_2)]}{W[2Pa^3 - P_{r1}(4a^3 - 3l_1a^2 - 3l_2a^2 + l_1^3 + l_2^3)]}$
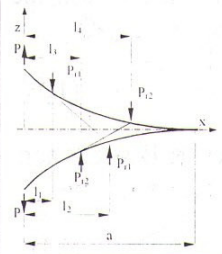	$C = \frac{8a^3}{WH^3E_x} - \frac{2[P_{r1}(4a^3 - 3l_1a^2 - 3l_2a^2 + l_1^3 + l_2^3) + P_{r2}(4a^3 - 3l_3a^2 - 3l_4a^2 + l_3^3 + l_4^3)]}{PWH^3E_x}$ $G_I = \frac{12P^2a^2}{W^2H^3E_x} - \frac{6Pa[P_{r1}(2a - l_1 - l_2) + P_{r2}(2a - l_3 - l_4)]}{W^2H^3E_x}$ $G_I = \frac{3P\delta a[2Pa - P_{r1}(2a - l_1 - l_2) - P_{r2}(2a - l_3 - l_4)]}{W[4Pa^3 - P_{r1}(4a^3 - 3l_1a^2 - 3l_2a^2 + l_1^3 + l_2^3) - P_{r2}(4a^3 - 3l_3a^2 - 3l_4a^2 + l_3^3 + l_4^3)]}$
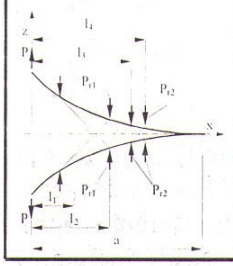	$C = \frac{8a^3}{WH^3E_x} - \frac{4[P_{r1}(4a^3 - 3l_1a^2 - 3l_2a^2 + l_1^3 + l_2^3) + P_{r2}(4a^3 - 3l_3a^2 - 3l_4a^2 + l_3^3 + l_4^3)]}{PWH^3E_x}$ $G_I = \frac{12P^2a^2}{W^2H^3E_x} - \frac{12Pa[P_{r1}(2a - l_1 - l_2) + P_{r2}(2a - l_3 - l_4)]}{W^2H^3E_x}$ $G_I = \frac{3P\delta a[Pa - P_{r1}(2a - l_1 - l_2) - P_{r2}(2a - l_3 - l_4)]}{W[2Pa^3 - P_{r1}(4a^3 - 3l_1a^2 - 3l_2a^2 + l_1^3 + l_2^3) - P_{r2}(4a^3 - 3l_3a^2 - 3l_4a^2 + l_3^3 + l_4^3)]}$

Fig.3. Derived equations for the DCB specimen including fiber-bridging.

4. STRESS DISTRIBUTION BEHIND THE CRACK-TIP

The stress distribution behind the crack-tip was investigated using the Winkler foundation model, as shown in Fig.4 [1]. The same model was applied by Ozdil and Carlsson, however only a correction factor for the compliance and fracture toughness of the glass/polyester DCB specimen was derived due to elastic foundation and crack-tip rotation. The displacement function was derived from the following governing differential equation:

$$\frac{d^4w(x)}{dx^4} + 4\lambda^4 H(x)w(x) = 0\,. \tag{18}$$

The complete solution of Eq(18). for the DCB specimen can be found in [1], using the proper boundary and matching conditions. The displacement field in the uncracked region can be expressed as:

$$w(x) = \frac{6P}{E_x wH^3\lambda^3}\left[\begin{array}{l} a\lambda\sin(\lambda x)\sinh(\lambda x) - \left(\frac{A-1}{2}\right)\sin(\lambda x)\cosh(\lambda x) + \\ + B\cos(\lambda x)\cosh(\lambda x) - \left(\frac{A+1}{2}\right)\cos(\lambda x)\sinh(\lambda x) \end{array}\right], \tag{19}$$

where

$$A=\left[\frac{\sinh^2(\lambda c)+\sin^2(\lambda c)}{\sinh^2(\lambda c)-\sin^2(\lambda c)}\right]+2a\lambda\left[\frac{\sinh(\lambda c)\cosh(\lambda c)+\sin(\lambda c)\cos(\lambda c)}{\sinh^2(\lambda c)-\sin^2(\lambda c)}\right], \quad (20)$$

$$B=a\lambda\left[\frac{\sinh^2(\lambda c)+\sin^2(\lambda c)}{\sinh^2(\lambda c)-\sin^2(\lambda c)}\right]+\left[\frac{\sinh(\lambda c)\cosh(\lambda c)-\sin(\lambda c)\cos(\lambda c)}{\sinh^2(\lambda c)-\sin^2(\lambda c)}\right], \quad (21)$$

$$\lambda=\frac{6^{1/4}}{H}\left(\frac{E_z}{E_x}\right)^{1/4} \quad (22)$$

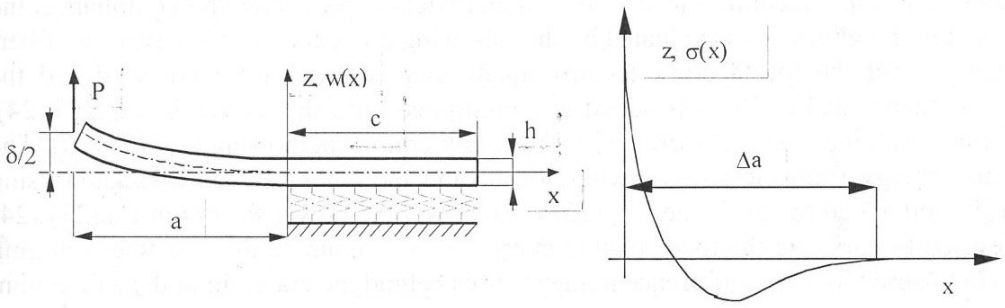

Fig.4. Elastic foundation model of the DCB specimen and stress distribution beyond the crack-tip.

Ozdil and Carlsson recommended a correction factor for the compliance and the fracture toughness based on the former Winkler foundation model:

$$C=\frac{8}{E_x w}\left(\frac{a}{H}\right)^3\left[1+1.92\left(\frac{H}{a}\right)\left(\frac{E_x}{E_z}\right)^{1/4}+1.22\left(\frac{H}{a}\right)^2\left(\frac{E_x}{E_z}\right)^{1/2}+0.39\left(\frac{H}{a}\right)^3\left(\frac{E_x}{E_z}\right)^{3/4}\right] \quad (23)$$

the fracture toughness can be determined by the derivative of Eq.(23) using Eq.(1):

$$G_I=\frac{12P^2a^2}{E_x w^2 H^3}\left[1+1.28\left(\frac{H}{a}\right)\left(\frac{E_x}{E_z}\right)^{1/4}+0.41\left(\frac{H}{a}\right)^2\left(\frac{E_x}{E_z}\right)^{1/2}\right]. \quad (24)$$

A similar expression was used by Kenane and Benzeggagh [13]. It is clear based on previous computations that this is not reasonable in high modulus composite DCB specimens. The stress and strain components in the z direction beyond the crack-tip can be expressed as:

$$\sigma_z(x)=E_z\varepsilon_z(x), \quad (25)$$

$$\varepsilon_z(x)=w(x)/(H/2). \quad (26)$$

According to the former equations the strain energy from the stress-field behind the crack-tip can be calculated as follows:

$$\Delta U_z=\frac{1}{2}\iiint_V\frac{\sigma_z^2(x)}{E_z}dV. \quad (27)$$

Since the stress component is independent from y and z, after integration of Eq.(27) respect to y and z yields:

$$\Delta U_z=\frac{1}{2}\frac{Hw}{E_z}\int_0^{\Delta a}\sigma_z^2(x)dx, \quad (28)$$

where Δa can be determined from the stress distribution, as shown in Fig.4. It was assumed that the strain energy resulted from the stress field behind the crack-tip is distributed in the area w*Δa. According to this the fracture energy can be calculated by dividing the strain energy by the area w*Δa:

$$\Delta G_I = \frac{1}{w}\frac{\Delta U_z}{\Delta a} = \frac{H}{2\Delta a E_z}\int_0^{\Delta a}\sigma_z^{\,2}(x)dx\,. \tag{29}$$

This fracture energy should be added to the results of Eq.(16). It must be noted that Δa is about 2-4 mm. According to the derived analytical expressions, the compliance and the fracture toughness was evaluated by the following procedure. In the case of no fiber-bridging (until the fourth crack length) equations given in Fig.1 were used and the fracture energy in Eq.(29) was added and multiplied with the factors in Eq.(23)-(24). The fiber-bridging was considered after the fourth crack length using Eq.(15)-(16). The fracture energy from the stress distribution behind the crack-tip was calculated using Eq.(29) and added to the former Eq.(15)-(16). Again the power factors in Eq.(23)-(24) were used to corrigate the total fracture energy. It was assumed that the fiber-bridging does not cause too much difference in the stresses behind the crack-tip in the z direction.

5. FINITE ELEMENT MODEL

The finite element code COSMOS/M 2.0 was used to carry out the analysis. Two-dimensional plain strain models were constructed to obtain numerical results for the mode-I interlaminar fracture toughness. The DCB specimens were meshed with four-noded plane strain elements (PLANE2D). TRUSS2D elements were utilized to represent the bridging fibers. In fact the J-integral is applicable only for isotropic models. Since the composites are anisotropic materials the models were constructed to include the anisotropy and the applicability of the J-integral, respectively. This problem was eliminated by creating a thin (0.15 mm) isotropic layer in the mid-plane of the specimen. It was assumed that the former modification does not affect the compliance and the fracture toughness of the specimen significantly. The J-integral was determined inside the former isotropic layer as shown in Fig.5. Inside the isotropic layer the modulus E_x was used, but it was verified and experienced, that the J-integral is not sensitive to the modulus, i.e. similar values were obtained for the fracture toughness using the through-the-thickness moduli E_z.

6. SPECIMEN DIMENSIONS, MATERIAL PROPERTIES AND LOAD/DISPLACEMENT DATA

For the present analysis the following elastic properties were assumed for the carbon/epoxy composite [2]: E_x=150 GPa, E_z=11 GPa, ν_{xz}=0.25, G=6 GPa and with specimen dimensions of w=20 mm, h=2 mm and initial crack length of a_0=45 mm. The same properties for the carbon/PEEK composite specimens [6]: E_x=124 GPa, E_z=10 GPa, ν_{xz}=0.25, G=5 GPa and specimen dimensions of w=20 mm, h=2.65 mm and a_0=20 mm.

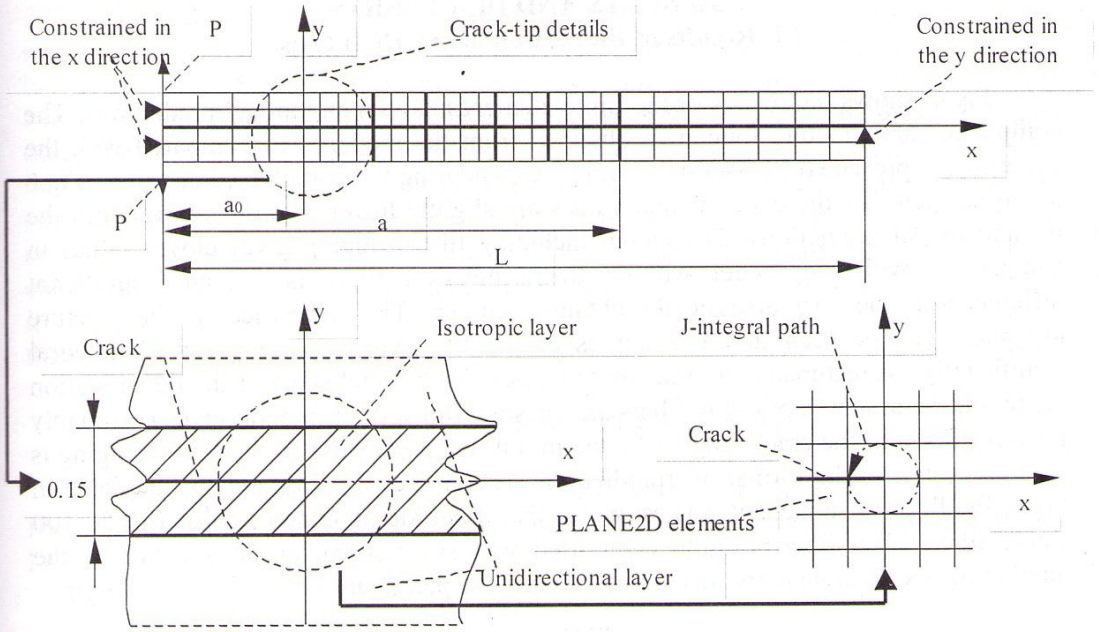

Fig.5.Finite element model of the DCB specimen, details of the crack-tip and J-integral path.

Note, that in the theory the model was investigated in the plane x-z, while the plain-strain FE model lies in the x-y plane. The through-the-thickness moduli was denoted by E_y is equal to E_z, the Poisson's ratio denoted as ν_{xz} is equal to ν_{xy} in the FE model. The bridging fiber bundles were described by the pure properties of carbon-fiber: E_{11}=235 GPa, G_{12}=24 GPa and ν_{12}=0.28, according to [14]. The load/displacement data is shown in Table 1 with the corresponding crack lengths.

Table 1.

Load/displacement data for the carbon/epoxy and carbon/PEEK composites.

Carbon/epoxy			*Carbon/PEEK*		
a [mm]	P [N]	δ [mm]	a [mm]	P [N]	δ [mm]
45	55.4	4.9	20	395	2.0
50	56.6	5.9	25	350	2.3
55	54	6.5	35	276	3.6
65	47.6	8.5	45	224	5.0
75	43	10.2	55	190	7.0
85	39.6	12.0	65	166	10.0
95	36	13.9	75	148	13.5
105	34.8	16.8	85	135	17.5
			95	125	21.5
			105	114	26.5
			115	112	33.0

7. RESULTS AND DISCUSSION

7.1. Results of the carbon/epoxy DCB tests.

Fig.6. shows the results of the finite element analysis and model predictions. The compliance and fracture toughness obtained from the models was compared with the experiments presented by Morais et al. [2]. Considering the compliance curves in Fig.6 it can be seen that the experimental values are slightly lower than the values from the FE and model predictions. The model including fiber-bridging gives closer values in comparison with the model without them, however there is not any significant difference in the two analytically obtained curves. The difference in the fracture toughness can be seen in the R-curves of the FE analysis. In Fig.6 the J-integral significantly overestimates the fracture toughness in the final stage of the delamination process if the assumed bridging fibers are missing. Since the J-integral gives reasonably good results until the crack length of a=65 mm it was assumed, that the fiber-bridging is the main cause of the former overpredictions. The corrected values are also depicted in Fig.6. In all the specimens it was estimated that the bridging bundles consist of 50-100 single fibers. The fiber-bridging form used was symmetrical arrangements and the number of fiber bundle pairs was increased until 4-5 pieces until the final crack length.

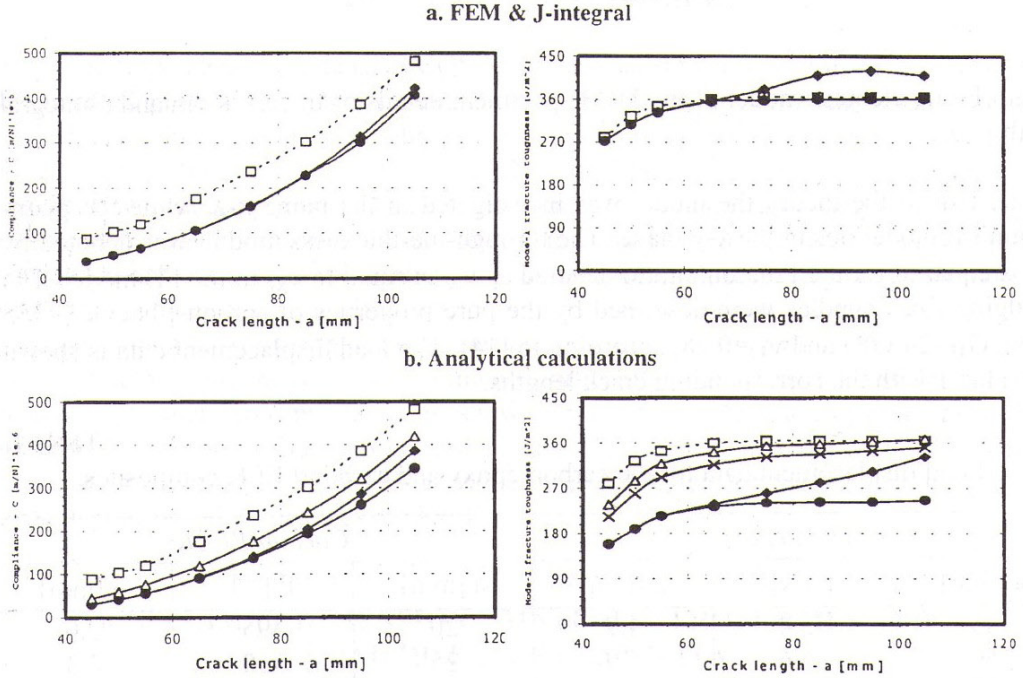

Fig.6. Compliance and R-curves for the carbon/epoxy DCB specimens. Experiments according to Morais et al. [□], models without fiber-bridging [♦], models including fiber-bridging [•], models including fiber-bridging and elastic foundation compliance correction [x], models including fiber-bridging, compliance correction and fracture energy from the stress field behind the crack-tip [Δ].

Morais et al. reported initiation toughness of G_{ICinit}=280 J/m^2 and steady-state toughness of about G_{ICss}=365 J/m^2. The current FE model including fiber-bridging gives

272.6 J/m^2 and 360 J/m^2 for the same quantities based on the J-integral. Considering the results of the simple beam theory without fiber-bridging no steady-state toughness can be determined. Since the beam theory is valid for composite specimens the experimentally measured and the curves of the beam theory should be parallel to each other, but in the final delamination stage the two curves almost coincide. The beam theory with bridging bundles partially eliminates this effect. The curves calculated considering the fiber-bridging and stress field behind the crack-tip give better correlation, but the best results were obtained in the case, including fiber-bridging, elastic foundation and the strain energy from the stress distribution behind the crack-tip. In the former case the elastic model gives G_{ICinit}=232.3 J/m^2 and G_{ICss}=362.1 J/m^2 for the initiation and steady-state toughness, respectively.

7.2. Results of the carbon/PEEK DCB tests.

Similar results were obtained in the case of carbon/PEEK composite specimens. Fig.7 illustrates the compliance and the mode-I fracture toughness calculated from the DCB tests.

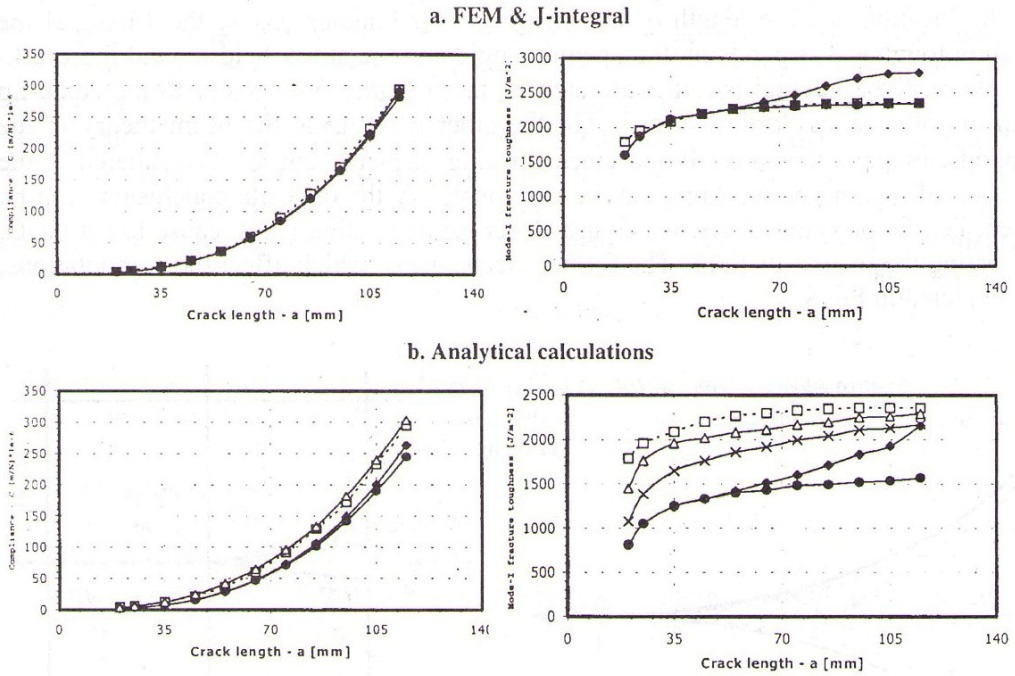

Fig.7. Compliance and R-curves for the carbon/PEEK DCB specimens. Experiments according to Hashemi et al. [□], models without fiber-bridging [♦], models including fiber-bridging [•], models including fiber-bridging and elastic foundation compliance correction [x], models including fiber-bridging, compliance correction and fracture energy from the stress field behind the crack-tip [Δ].

Excellent results were presented for the compliance by both the finite element and analytical models. The fracture toughness values obtained by finite element calculations again are higher than the measured ones after the crack length of 55 mm. The

application of symmetrically arranged bridging fiber bundles leads to reasonable fracture energy values. The FE model reports G_{ICinit}=1595 J/m^2 and G_{ICss}=2347.6 J/m^2 against the experimentally obtained G_{ICinit}=1790 J/m^2 and G_{ICss}=2360 J/m^2 values, presented by Hashemi et al. [6]. Considering the analytically obtained fracture energies the same conclusions can be taken as in the carbon/epoxy DCB specimens. No steady-state toughness exists until the bridging fiber bundles are missing. The correction due to elastic foundation and stress field behind the crack-tip is necessary to be considered for the best results. The corresponding initiation and steady-state toughness values: G_{ICinit}=1451 J/m^2 and G_{ICss}=2260 J/m^2, respectively. However both the FE and elastic models underpredicted the initiation fracture toughness, these results can be regarded as good correlation with the experiments. The former underprediction can be associated to the fact that the beam theory is strictly valid only for infinitely long crack lengths.

7.3. General discussion.

However both the FE model including fiber-bridging and the elastic model completed with other corrections due to elastic foundation and fiber-bridging gives more realistic results, the J-integral and the theoretical models are differently affected by the location and the length of the bridging fiber bundles. Using the J-integral the fracture toughness depends on the opening angle and the stress field around the crack-tip. Hence the J-integral is rather affected by the bridging fibers close to the crack-tip than the other ones, further from it. On the other hand using the beam theory in the applied equations the force, P and crack opening displacement, δ is considered at the location of loading point. Applying the current theory the opposite conclusions can be taken, i.e. the bridging fibers, which are closer to the loading point, cause lower COD, correcting the overpredictions. The former mechanisms, which affect the computations, are depicted in Fig.8.

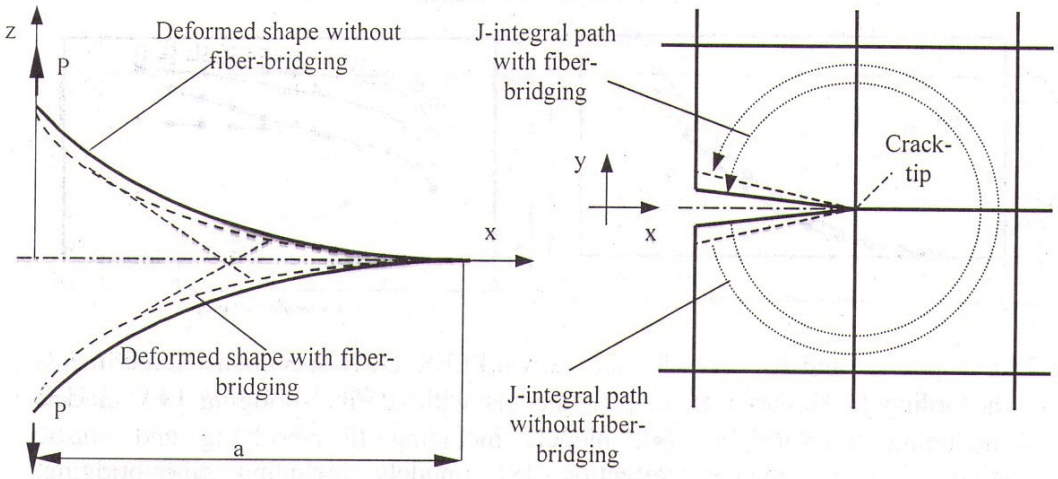

Fig.8. Deformed shape and crack-tip details with and without fiber-bridging.

The fracture energy, calculated from the stress field behind the crack-tip was found to be increasing with the crack length. This was also proved by finite element

calculations, however in the stress values at the crack-tip significant differences were experienced. The FE model gives 400-500 MPa maximal value for the stress component σ_z, while the analytical model shows only 8-10 MPa for the same quantity. This overprediction using the FE model can be the consequence of the fact, that the crack-tip is singular point in the stress field, and stress concentration can occur by refining the FE mesh. In the theory there is no stress singularity.

8. CONCLUSIONS

Unidirectional carbon/epoxy ($[0°]_{24}$) and carbon/PEEK ($[0°]_{40}$) DCB specimens were investigated analytically and numerically. The fiber-bridging phenomenon was analysed based on linear elastic beam theory and generalized closed-form equations were derived for the compliance and for the fracture toughness. Previous computations showed that the simple beam theory gives very poor results for high axial modulus composite DCB specimens in comparison with the experimentally measured fracture toughness. The stress field behind the crack-tip was found to be another source of fracture energy, which should be accounted to obtain reasonably good fracture energy values. Elastic foundation correction factors due to crack-tip rotation were also used. The best results were obtained by the models, which accounts for fiber-bridging, elastic foundation and the stress field behind the crack-tip. The fracture toughness was evaluated fully analytically and very good predictions were made. Numerical computations were also carried out based on the J-integral. The finite element analyses also showed large overpredictions in comparison with the experimental fracture tests. After the fiber-bridging phenomenon was considered result showed excellent correspondence with the experiments for both the compliance and the mode-I interlaminar fracture toughness. The following conclusions were taken:

- the beam theory shows, the fiber-bridging cause a term in the specimen compliance, which has the quadratic and cubic power of the crack length;
- if the fiber-bridging is not considered, the beam theory, as well as the J-integral overpredicts the fracture energy based on the experimental load-displacement curves;
- the stress field behind the crack tip should be accounted ass another source of fracture energy;
- the beam theory formulas are affected by fiber-bridgings, closer to the loading point significantly, while the J-integral is rather affected by the fiber bundles closer to the crack tip.

The fiber-bridging phenomenon is also observable in laminated angle-ply composites. There are other practical problems in composite DCB specimens considering the fiber-bridging. For instance the nonuniform distribution of the fracture energy along the specimen width, curved crack front, the effects of stacking sequence on the fiber-bridgings, etc. These problems have planned to be solved by us in the future.

9. REFERENCES

1. Ozdil F., Carlsson L.A. Beam analysis of angle-ply laminate DCB specimens. Composites Science and Technology, 1999, v.59, pp.305-315.
2. Morais A.B., Moura M.F., de, Marques A.T., Castro P.T. Mode-I interlaminar fracture of carbon/epoxy cross-ply laminates. Composites Science and Technology, 2002, v.62, pp.679-686.
3. Suppakul P., Bandyopadhyay S. The effect of weave pattern on the mode-I interlamianr fracture energy of E-glass/vinyl ester composites. Composites Science and technology, 2002, 62, pp.709-717.
4. Shen F., Lee K.H., Tay T.E. Modelling delamination growth in laminated composites. Composites Science and Technology, 2001, v.61, pp.1239-1251.
5. Dubois F., Keunings R. DCB testing of thermoplastic composites: a non-linear micro-macro numerical analysis. Composites Science and Technology, 1997, v.57, pp.437-450.
6. Hashemi S., Kinloch J., Williams J.G. The effects of geometry, rate and temperature on mode I, mode II and mixed-mode I/II imterlaminar fracture toughness of carbon-fibre/poly(ether-ether ketone) composites. Journal of Composite Materials, 1990, v.24, pp.918-956.
7. Hashemi S., Kinloch J., Williams J.G. Mechanics and mechanisms of delamination in a poly(ether sulphone)-fibre compsoites. Composites Science and Technology, 1989, N378, pp.429-462.
8. Dahlen C., Springer G.S. Delamination in composites under cyclic loads. Journal of Composite Materials, 1994, v.28, pp.732-781.
9. Broek D. Elementary engineering fracture mechanics. Martinus Nijhoff Publishers, The Hauge, 1982.
10. Tanzawa Y., Watanabe N., Ishikawa T. FEM simulation of a modified DCB test for 3-D orthogonal interlocked fabric composites. Composites Science and Technology 2001, v.61, pp.1097-1107.
11. Tanzawa Y., Watanabe N., Ishikawa T. Interlaminar fracture toughness of 3-D orthogonal interlocked composites. Composites Science and Technology 1999;59;1261-1270.
12. Heck A. Introduction to Maple. Springer-Verlag 1993.
13. Kenane M., Benzeggagh M. L. Mixed-mode delamination fracture toughness of unidirectional glass/epoxy composites under fatigue loading. Composites Science and Technology, 1997, v.57, pp.597-605.
14. Fiedler B., Hojo M., Ochiai S., Schulte K., Ochi M. Finite-element modeling of initial matrix failure in CFRP under static transverse tensile load. Composites Science and Technology, 2001, v.61, pp.95-105.

Поступила в редакцию 30 сентября 2002 года.